Robotica: (2020) volume 38, pp. 1478–1494. © Cambridge University Press 2019
doi:10.1017/S0263574719001589

Implementation of a Reconfigurable Robot to Achieve Multimodal Locomotion Based on Three Rules of Configuration

Faliang Zhou†, Xiaojun Xu†*, Haijun Xu†, Yukang Chang†, Qi Wang‡ and Jinzhou Chen¶

† *College of Intelligence Science and Technology, National University of Defense Technology, Changsha 410073, China.*
E-mails: Shinny08@163.com, xuhaijun_1999@163.com, 15575166773@163.com
‡ *School of Information and Software Engineering, University of Electronic Science and Technology of China, Chengdu 610054, China.*
E-mail: 2017220301007@std.uestc.edu.cn
¶ *China Astronaut Research and Training Center, Beijing 100094, China.*
E-mail: chenjinzhouacc@163.com

(Accepted October 9, 2019. First published online: November 25, 2019)

SUMMARY
In this paper, we focus on the configuration design of a reconfigurable robot that merges the functions of wheels, tracks, and legs together. A deformable rim is utilized to make the robot wheel reconfigurable to change its locomotion mode. Three rules of configuration design to achieve reconfiguration between different modes are proposed: (1) in wheel mode, the track wheel set should be hidden inside the wheel rim; (2) in track/leg mode, the folded wheel rim should be hidden inside the caterpillar loop; (3) the circumference of the wheel rim in wheel mode should be equal to the length of the track ring in track mode. According to these rules, the configuration of the deformable rim, track wheel set, and telescopic spoke are analyzed and designed. A prototype of the reconfigurable wheel is fabricated by three-dimensional printing, and its functions of locomotion in different modes, the switch between different modes, and its load-bearing ability are tested, verifying the effectiveness of the configuration design. Furthermore, a prototype of the reconfigurable robot is manufactured by computerized numerical control (CNC) machining to verify the structural design of the reconfigurable wheel. Compared to traditional hybrid robots with separate wheels, tracks, and legs, this reconfigurable design lends the multimodal robot both excellent terrain adaptability and a compact structure; thus, it can be widely used as a universal mobile platform in search and rescue missions and explosive object disposal missions.

KEYWORDS: Reconfigurable robot; Deformable rim; Multimodal locomotion; Configuration rules.

1. Introduction

Search and rescue (SAR) and explosive object disposal (EOD) missions are usually dangerous. Moreover, such tasks are usually accompanied by structural damage, which means the working field is tough and narrow, making it difficult to reach by human.[1–4] Nowadays, small unmanned mobile robots are becoming more widely used in such missions for two main reasons. Firstly, replacing

* Corresponding author. E-mail: xuxiaojunmail@sina.com

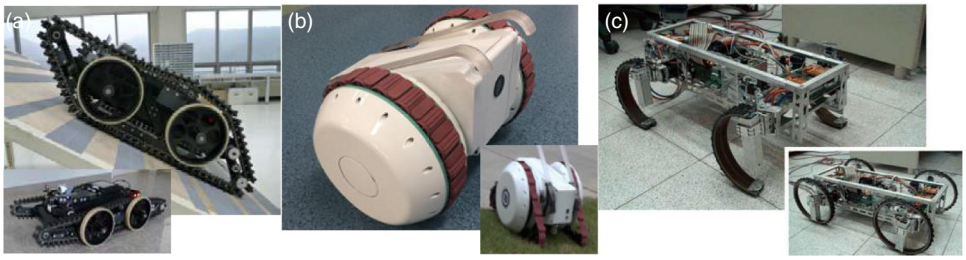

Fig. 1. Present hybrid robots: (a) hybrid robot with separate wheels and tracks; (b) wheel–track robot with a length-variable band; (c) wheel–leg robot with a semi-circle leg.

human with robots can efficiently reduce or even avoid casualties. Secondly, the small size of the robot makes it easier to get in those narrow spaces. In view of the urgency of such tasks and the unpredictable terrain that may be encountered, robots are required to have terrain adaptability and rapid maneuverability in an unstructured environment.[5–8]

Currently, wheeled robots are most commonly used for their ability to move quickly and efficiently on flat terrain. However, their shortcoming of poor terrain adaptability is an issue in the wild environment. Therefore, a lot of research has been conducted around the world to change the shape of the wheel rim so as to alter the way a robot comes into contact with the ground, thus improving its terrain adaptability. A simple method is to assemble separate wheels, tracks, and legs together; however, this often results in increased structural complexity and motion interference between different modes[9–13] (see Fig. 1(a)). Therefore, research focusing on robots that achieve multimodal locomotion via transformation has been popular in recent years. These robots can be classified into two categories—one that converts between continuous point contact of the wheel and continuous line contact of the track, so that the robot combines the advantages of both wheels and tracks, and another that can switch between continuous point contact of the wheel and discrete point contact of the leg, so that the robot possesses the advantages of both wheels and legs.

Among the wheel–track hybrid robots, Je-sung Koh et al. developed a multimodal robot with a flexible wheel made of paper and film.[14,15] Controlled by a novel spoke actuated by shape memory alloy, the shape of the flexible wheel can switch from a circle to an ellipse to enlarge the contact area between the wheel and the ground. Another solution is switching the round wheel to a triangle track, which hides the track wheel set in the huge wheels in wheel mode and stretches it out in track mode. For example, Jianbing Hu et al. presented a wheel–track transformable robot with a variable-length caterpillar band to fit the track ring's length change during the transformation[16] (see Fig. 1(b)). However, the stretchable caterpillar has the disadvantage of being easy to slip off. To improve this design, another two solutions have been proposed. One of them folds the length-fixed caterpillar belt inside the robot wheel and expands it out to make contact with the floor in track mode;[17] the other robot, presented in ref. [18], utilizes a diameter-variable driving wheel to adapt to the length change of the caterpillar band during transformation. The caterpillar bands of these two robots both have a fixed length, which reduces the possibility of slipping off but is employed at the expense of a simple structure.

As for wheel–leg hybrid robots, the switch from wheel mode to leg mode is usually achieved by segmenting a whole wheel rim to several arc legs, so that the robot can move with a walking leg. For example, Jui-Jen Chou et al. from National Taiwan University proposed a wheel–claw hybrid transformable robot whose wheels are spliced by two "S"-shaped half-wheels.[19] The two half-wheels can be overlapped into claws when needed. In this way, the contact type between the robot and the ground changes from continuous points to discrete points, so the robot can climb large obstacles like a legged robot. Xinbo Chen et al. presented a walking wheel robot which transforms a round wheel to a legged wheel by enlarging the wheel diameter. Yu She introduced a robot which switches from a circled wheel to a spoke–leg by the slide of crank linkages in the axial direction.[20] Kenjiro Tadakuma invented a novel wheel–leg robot in ref. [21] which can change a circled wheel into a three-jointed long leg by separating the rim into three segments and jointing them. The Wheel Transformer also cuts the wheel rim into three arc segments.[22,23] The difference is that its round wheel transforms into a three-leg wheel. Rajesh Elara Mohan et al. developed a shape-shifting rolling–crawling robot that can unfold a wheel to two semi-circle legs.[24,25] Quattroped and TurboQuad models switch their

https://doi.org/10.1017/S0263574719001589 Published online by Cambridge University Press

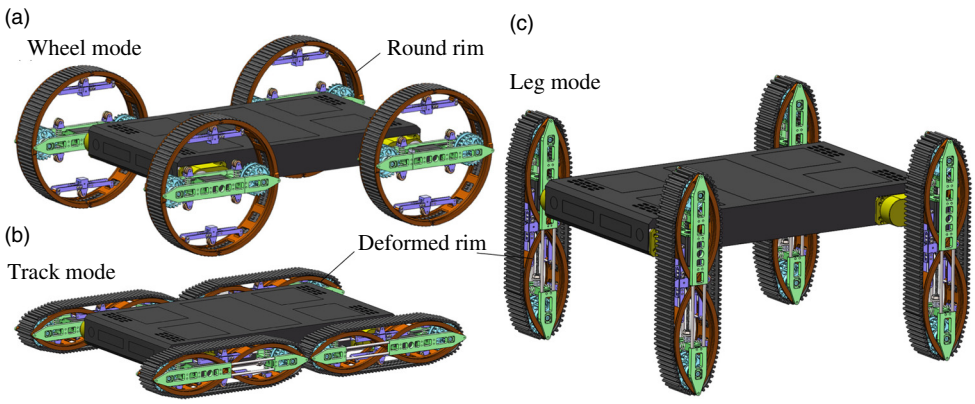

Fig. 2. 3D mode of the reconfigurable robot.

locomotion mode by folding the morphology of the circle wheel into one semi-circle leg[26–29] (see Fig. 1(c)).

Although there are so many designs implementing multimodal movement, they can only change the configuration between wheels and tracks or wheels and legs. Therefore, we propose a reconfigurable design which realizes the locomotion mode switch between wheels, tracks, and legs through changing the shape of the rim (see Fig. 2). On flat and firm roads, the rim is round and the robot works in ordinary wheel mode. On swampy and slippery terrains, the rim can be squeezed and folded and the configuration of the round wheel can be converted to an oblate track. Furthermore, the oblate track can rotate around the wheel hip as a leg to climb up steps and stairs. In this way, the reconfigurable wheel integrates the advantages of a wheel, track, and leg together, so that the robot can select the most efficient locomotion mode according to different terrains. Compared to traditional hybrid robots with separate wheels, tracks, and legs, this reconfigurable design provides the robot with both excellent terrain adaptability and a compact mechanism structure.

The general design concept and configuration rules of the reconfigurable robot to achieve multimodal locomotion are introduced in Section 2. In Section 3, the configuration design process of the deformable wheel rim and track wheel set is described in detail. Section 4 presents the mode switch process modeling and analysis of the reconfigurable wheel. A three-dimensional (3D)-printed prototype of the reconfigurable wheel is tested in Section 5 to verify the switch performance between different modes. In addition, a prototype of the reconfigurable robot is fabricated by computerized numerical control (CNC) machining to verify the locomotion function of the design. Section 6 gives a summary of the work of the full text and a simple outlook for follow-up work.

2. Configuration Rules to Achieve Multimodal Locomotion

2.1. Mode switch concept design

Our original intention was to improve the mobility of wheeled robots without significantly complicating the mechanical structure. The best way is to realize multimodal locomotion by mechanism reconfiguration instead of assembling individual wheels, tracks, and legs together. According to our design, the conversions between wheels, tracks, and legs are the transition of the robot's contact type against the ground, which can be achieved by the deformation of the wheel rim to make the robot reconfigurable as shown in Fig. 3. Assuming that the wheel rim is deformable and transforms to a flat ring, the round wheel (see Fig. 3(a)) switches to a flat track, which means a continuous point contact is converted to a continuous line contact (see Fig. 3(b)). And if the flat track rotate around the hip joint, it works as a rolling leg (see Fig. 3(c)), which means the continuous line contact is converted to a discrete point contact. Therefore, the wheeled robot can switch to track mode by the forward deformation of the wheel rim, and the stick leg can transform back to wheel mode by the inverse deformation. In this way, the reconfigurable robot can change its locomotion mode among wheels, tracks, and legs according to the terrain situation.

The deformation ability of the wheel rim is fundamental to the reconfiguration and multimodal locomotion of the robot. In addition to this, some other rules should also be followed. In the following

https://doi.org/10.1017/S0263574719001589 Published online by Cambridge University Press

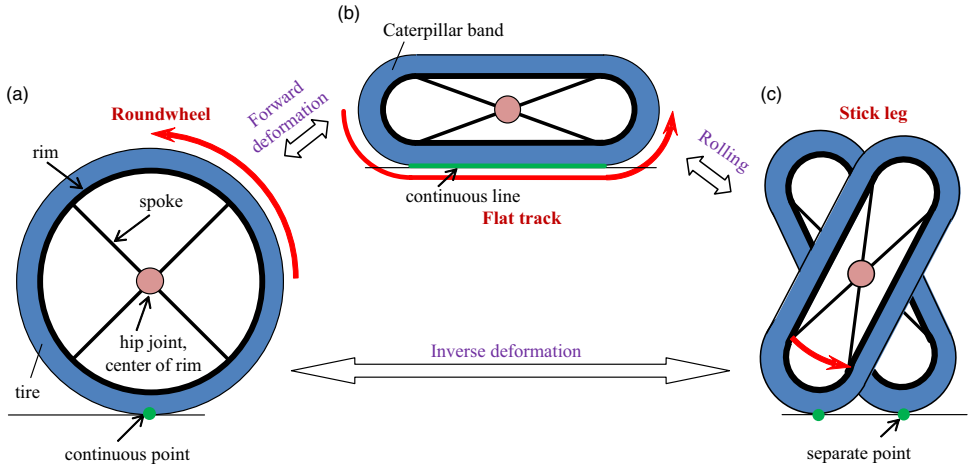

Fig. 3. Mode switch concept of a reconfigurable wheel.

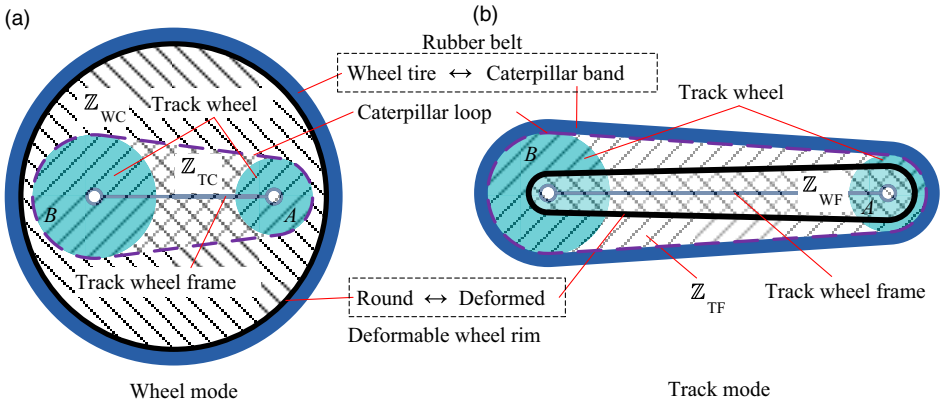

Fig. 4. Configuration rules diagram of the mode switch.

text, configuration rules and candidate options of the reconfigurable wheel are discussed based on different combinations of track wheel set and foldable rim.

2.2. *Configuration rules analysis*

The locomotion mode switch represents a conversion between different types of ground contact. As shown in Fig. 4(a), in wheel mode, the track wheels mounted on the track wheel frame are hidden inside the wheel rim to avoid contact with the ground. And the rubber belt surrounds the round rim, working as a tire. When transforming to track mode through the deformation of the rim (see Fig. 4(b)), the track wheels are stretched out and propped up against the rubber belt to make it works as a caterpillar band, the shape of which is the same as that of the caterpillar loop (i.e., the shortest enveloping loop that surrounds all the track wheels inside).

Since the circumference of the flexible rim remains unchanged during the deformation, the layout and extension principle of the track wheel set must meet certain constraints:

$$\begin{cases} \mathbb{Z}_{\mathrm{TR}} \subseteq \mathbb{Z}_{\mathrm{WR}} \\ \mathbb{Z}_{\mathrm{TD}} \supseteq \mathbb{Z}_{\mathrm{WD}} \\ l_{\mathrm{TD}} = l_{\mathrm{WR}} \end{cases} \tag{1}$$

where $\mathbb{Z}_{\mathrm{WR}}$ and $\mathbb{Z}_{\mathrm{TR}}$ denote the coverage zone of the wheel rim and caterpillar loop when the deformable rim is round, respectively. Meanwhile, $\mathbb{Z}_{\mathrm{WD}}$ and $\mathbb{Z}_{\mathrm{TD}}$ represent the coverage zone of the wheel rim and caterpillar loop when the rim is deformed, respectively. l_{TD} is the circumference of the caterpillar loop in track mode and l_{WR} is the circumference of the wheel rim.

https://doi.org/10.1017/S0263574719001589 Published online by Cambridge University Press

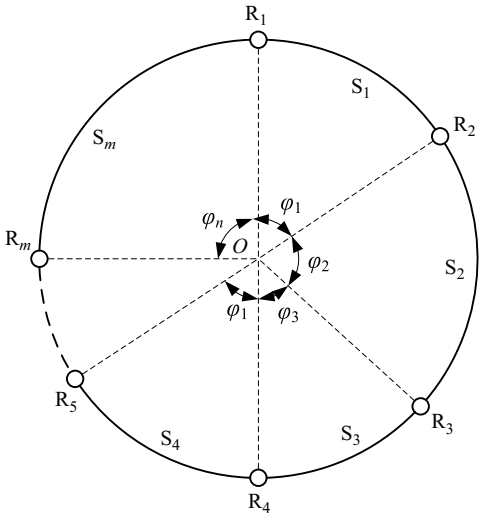

Fig. 5. Closed-single-loop-chain configuration of the deformable rim.

When the deformable rim is round, the coverage zone of the track circuit should be included in the coverage zone of the wheel rim, corresponding to the first formula in Eq. (1). At this time, the rubber belt is supported by the wheel rim and works as a wheel tire. The reconfigurable wheel makes contact with the ground at continuous points, which means it works in wheel mode.

During the transformation of the deformable rim, the track wheels gradually expand out of the wheel rim and stretch up the rubber belt. When the wheel rim is folded, the rubber belt is separated from the wheel rim and supported by the track wheels. Furthermore, the coverage zone of the folded wheel rim should be included in the coverage zone of the track circuit to avoid interference with the rubber belt, corresponding to the second formula in Eq. (1). At this time, the reconfigurable wheel works in track mode and the rubber belt works as a caterpillar belt. In this way, the continuous point contact is converted to a continuous line contact.

3. Configuration Design of the Reconfigurable Wheel

3.1. Deformable rim configuration design

In this paper, the deformation of the wheel rim is realized by cutting the rim into several segments and jointing their ends to form a chain. As shown in Fig. 5, the configuration of the deformable wheel rim is a planar single-loop-chain mechanism. S_i and R_i denote the i^{th} arc rim segment and revolute pair, respectively. Some segments may have the same apex angle, for example, S_1 and S_4, which are defined as the same type of segment. Therefore, the configuration needs to meet the following constraints:

$$\begin{cases} m = \sum_{j=1}^{n} p_j \\ \sum_{j=1}^{n} p_j \varphi_j = 2\pi \end{cases} \tag{2}$$

where p_j and $\varphi_j (j = 1, \ldots, n)$ represent the quantity and apex angle of the j^{th} type of arc rim segment, respectively. m and n denote the total quantity and type quantity of the segments that compose the deformable rim, respectively.

As a planar linkage mechanism, the degree of freedom (DOF) of the deformable rim can be calculated by:[30]

$$F = 3q - (2q_{\text{l}} + q_{\text{h}}) = 3(m-1) - 2m = m - 3 \tag{3}$$

where q indicates the number of moving links, and $q = m - 1$. q_l is the number of lower pairs and q_h is the number of higher pairs in the deformable wheel rim. Since only revolute pairs which belong to the lower pair joint are utilized in the configuration, then $q_l = m$, $q_h = 0$.

https://doi.org/10.1017/S0263574719001589 Published online by Cambridge University Press

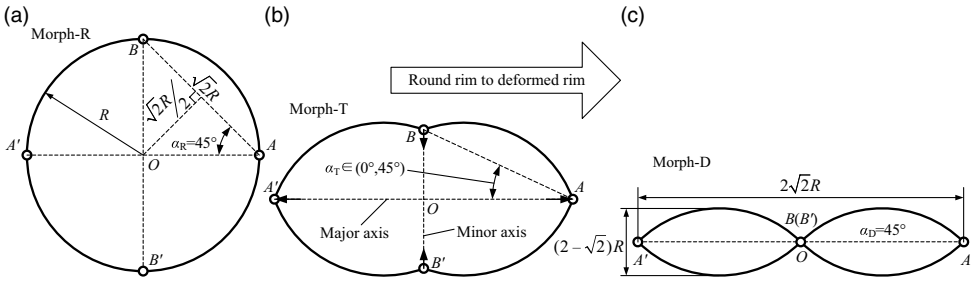

Fig. 6. Different morphologies of a four-segment deformable rim.

This means that as long as m is no less than 4, the wheel rim can be deformed. And there are an infinite number of configurations that meet the requirement. However, the larger the number of segments is, the more mode switch driving spokes are required to control the shape of the deformable wheel rim, and the more complex the reconfigurable wheel structure is. According to the three rules of configuration in Eq. (1), in wheel mode, the deformable wheel rim is always rounded and will not affect the wheel's locomotion despite different numbers of segments. In track mode, the deformed wheel rim is hidden inside the caterpillar loop and does not contact with the caterpillar band, nor does it affect the track's locomotion. Besides, the legged locomotion is achieved by the rotation of the whole reconfigurable wheel in track mode, which means that the configuration differences of the deformable rim have no influence on the locomotion of leg mode either. It can be seen that the number of segments does not affect the locomotion of the reconfigurable wheel in any mode, but only affects the structure complexity of the deformable wheel rim and the mode switch driving spokes. Therefore, we set $m = 4$ to simplify the structure design (see Fig. 6). Then $n = 1$, $p_1 = 4$, and $\varphi_1 = \pi/2$, which presents the simplest configuration of the deformable wheel rim.

In wheel mode, the morphology of the deformable rim is round (Morph-R, see Fig. 6(a)). When the robot needs to move in track mode or leg mode, the round rim can deformed to a "∞"-shaped ring (Morph-D, see Fig. 6(c)). During this mode switch process, which is called Morph-T (see Fig. 6(b)), the length of *AA'* (called the major axis) increases while *BB'* (called the minor axis) decreases. Setting the wheel rim radius to R, it is easy to figure out that the variation range of the long axis' length is $l_{AA'} \in [2R, 2\sqrt{2}R]$, while that of the short axis' length is $l_{BB'} \in [0, 2R]$. In Morph-D, the length and height of the deformed wheel rim are $2\sqrt{2}R$ and $(2 - \sqrt{2})R$, respectively.

3.2. Track mode configuration analysis

Based on above analysis of the configuration rules of the reconfiguration wheel, it was found that the configuration of the caterpillar loop is the key factor that decides whether the track mode can work normally. According to the present research,[31] there are three types of classical layouts for a caterpillar loop: (1) both the driving and idler wheels make contact with the ground, working as loading wheels as well; (2) only the driving wheel makes contact with the ground, also working as a loading wheel, while the idler wheel breaks away from the ground; (3) neither the drive nor the idler wheel makes contact with the ground and both of them break away from the ground.

Additionally, the configuration symmetry and balance of the caterpillar loop should be taken into consideration for two reasons. One is to simplify the structure design and fabrication. The other is to take into account the dynamic balance of the reconfigurable wheel in wheel mode. Thus, three different configurations of the caterpillar loop are proposed, as shown in Fig. 7, where the dashed lines represent wheel mode and the solid lines represent track mode. r_1, r_2, and r_3, respectively, indicate the radii of the track driving wheels and the loading wheels, which may be equal or unequal among different caterpillar loop configurations. h_2 and d_2, h_3 and d_3, respectively, present the distance between the idler wheel and coordinates in second and third configuration. l_1, l_2, and l_3 mean the center distance of the driving wheel and the idler wheel in the three kinds of caterpillar loop, respectively.

Figure 7(a) corresponds to the first layout of the caterpillar loop, which is rod-shaped with both the driving wheel and idler wheel on the ground. Figure 7(b) is a centrally symmetric parallelogram,

https://doi.org/10.1017/S0263574719001589 Published online by Cambridge University Press

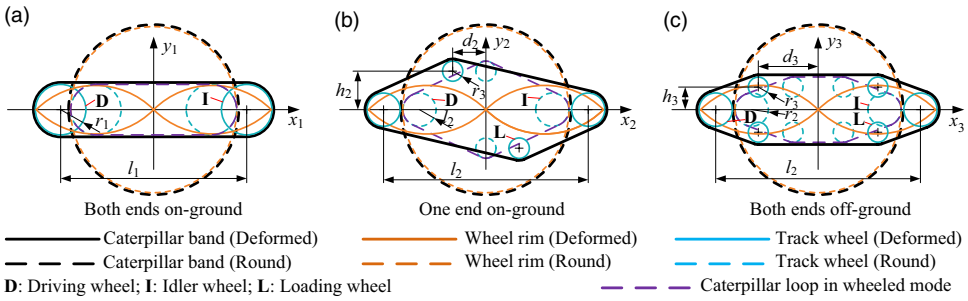

Fig. 7. Different configurations of the caterpillar loop.

corresponding to the second layout of the caterpillar loop with one end (i.e., the idler wheel) off the ground. Figure 7(c) corresponds to the third layout, which is fusiform with both the driving wheel and idler wheel off the ground. In wheel mode, when the deformable rim is round (shown as dashed lines), the caterpillar loop (shown as purple dashed lines) of all the three kinds of reconfigurable wheels is included in the wheel rim and symmetrically placed around the center. Furthermore, when determining the position of the track wheels in track mode, the caterpillar band is not allowed to contact with the deformed wheel rim. Besides, the length of the caterpillar loop is considered to be equal to the original length of the wheel rim in wheel mode. Take the first kind of configurable wheel as an example, the structure dimensions should obey the following constraints according to the configuration rules:

$$\begin{cases} 2\sqrt{2}R < 2r_1 + l_1 \\ \left(1 - \frac{\sqrt{2}}{2}\right) R < r_1 \\ 2\pi R = 2\pi r_1 + 2l_1 \end{cases} \tag{4}$$

where R means the radius of the deformable wheel rim. To simplify the design, the driving wheel and the idler wheel have the equal radius r_1.

Therefore, the three rules in Eq. (1) are satisfied. The value ranges of the track wheel radius r_1 and center distance l_1 can be obtained:

$$\begin{cases} \frac{2-\sqrt{2}}{2} R < r_1 < \frac{\pi - 2\sqrt{2}}{\pi - 2} \\ \frac{2\sqrt{2}-2}{\pi-2}\pi R < l_1 < \frac{\sqrt{2}}{2}\pi R \\ l_1 = \pi(R - r_1) \end{cases} \tag{5}$$

If $R = 100$ mm is set, there is

$$\begin{cases} 27.4 < r_1 < 29.3 \\ 222.1 < l_1 < 227.9 \\ l_1 = \pi(R - r_1) \end{cases} \tag{6}$$

It can be seen that, when R is constant, there are infinite number of available solutions of r_1 and l_1. Since the variation ranges of these two parameters are both quite small, it is desirable to set $r_1 = 28$ mm, $l_1 = 226$ mm. By utilizing the similar method, the configuration dimensions of the latter two kinds of caterpillar loops, such as $r_2 = 20$ mm, $r_3 = 12$ mm, $h_2 = 46$ mm, $d_2 = 40$ mm, $h_3 = 32$ mm, and $d_3 = 76$ mm, can also be calculated, of which the detailed solution process can be found in our previous published paper.[32]

For track mode, the performances of obstacle-crossing ability and load-bearing ability are mainly concerned. According to ref. [33], these two indexes are positively correlated with the off-ground height of the idler wheel and the grounding length of the track, respectively. As shown in Fig. 8, theoretically, the maximum step-climbing height of the track equals the off-ground height of the idler wheel. To simplify the design process, the track wheels of the idler wheel off-ground configuration (see Fig. 8(b)) and the both driving wheel and idler wheel configuration (see Fig. 8(c)) are set with the same size.

https://doi.org/10.1017/S0263574719001589 Published online by Cambridge University Press

Table I. Performance comparison of different configurations (unit: mm).

Category	Both ends on-ground	One end off-ground	Both ends off-ground
Grounding length (load ability)	226 (good)	166 (medium)	152 (poor)
Off-ground height (obstacle ability)	28 (poor)	75 (good)	44 (medium)

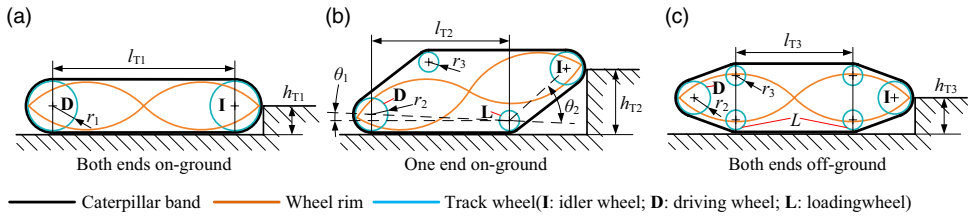

Fig. 8. Grounding length and off-ground height diagram of different configurations.

Therefore, the grounding length and off-ground height of these three kinds of caterpillar loops, l_{T1}, h_{T3}, l_{T2}, h_{T2}, l_{T3}, h_{T3} can be calculated by:

$$\begin{cases} l_{T1} = l_1 \\ h_{T3} = r_1 \end{cases}, \begin{cases} l_{T2} = \sqrt{\left(\frac{l_2}{2} + d_2\right)^2 + h_2^2 - (r_2 - r_3)^2} \\ h_{T2} = r_3 + \sin(\theta_2 - \theta_1)\sqrt{\left(\frac{l_2}{2} - d_2\right)^2 + h_2^2} \end{cases}, \begin{cases} l_{T3} = 2d_3 \\ h_{T3} = r_3 + h_3 \end{cases} \tag{7}$$

where θ_1, θ_2 can be described by:

$$\begin{cases} \theta_1 = \arcsin \frac{r_2 - r_3}{\sqrt{\left[(\frac{l_2}{2} + d_2)^2 + h_2^2\right]}} \\ \theta_2 = \pi - \arccos \frac{2(h_2^2 + d_2^2) - l_2^2/2}{2\sqrt{\left[(\frac{l_2}{2} + d_2)^2 + h_2^2\right]\left[(\frac{l_2}{2} - d_2)^2 + h_2^2\right]}} \end{cases} \tag{8}$$

According to Eq. (8), the grounding length and off-ground height of different caterpillar loops can be figured, as shown in Table I. The longer contact line presents a smaller pressure against the ground, which indicates a better load-bearing performance. A higher off-ground height of the idler wheel means a bigger step that the robot can climb up. It can be seen that the both ends on-ground configuration (Fig. 8(a)) have the longest contact line with the ground while the shortest off-ground height of the idler wheel among the three categories. This means that this kind of track configuration has a good load-bearing ability but a poor ability to overcome obstacles. The both ends off-ground configuration (Fig. 8(b)) own the biggest off-road distance of the idler wheel and a shorter contact line with the ground. This means that this kind of track configuration has an excellent ability to overcome obstacles but a poor ability to bear load. The one end off-ground configuration (Fig. 8(c)), in which the off-road distance is between the above two and the contact line length is the shortest, has a medium ability to overcome obstacles but the poorest load-bearing ability among the three categories. By comparison, it was found that the second category of reconfigurable wheel has the best comprehensive locomotion performance, the first category follows, and the third is worst. Since the obstacle-climbing ability can be enhanced by the rolling of the deformed reconfigurable wheel in leg mode, and the end on-ground type requires the smallest number of track wheels and the simplest structure, the first category of caterpillar loop is chosen to be further studied in this paper.

4. Mode Switch Process Modeling and Analysis

In the last section, the configuration of the deformable wheel rim and the track wheel set were designed and analyzed. To enable the reconfigurable wheel transform successfully between different locomotion modes, a deformation driving spoke is needed to drive the shape change of the deformable rim (see Fig. 9). According to Eq. (3), the four-segment foldable rim is a single-DOF

https://doi.org/10.1017/S0263574719001589 Published online by Cambridge University Press

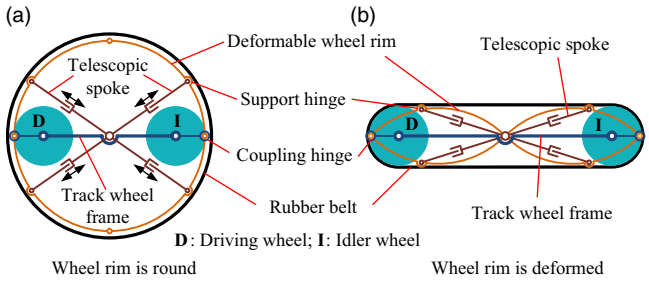

Fig. 9. Mode switch diagram of the reconfigurable wheel.

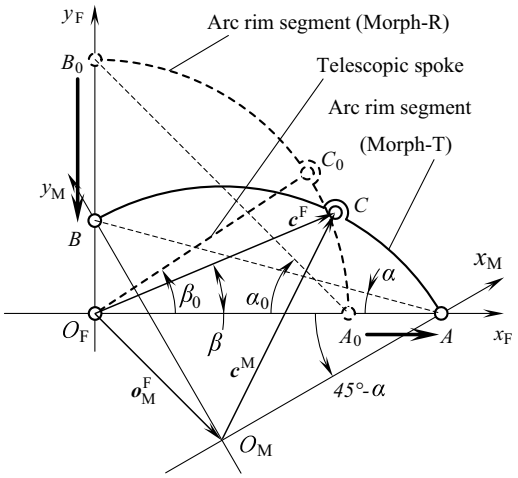

Fig. 10. Kinematic diagram of the mode switch process.

planar mechanism, meaning that the deformation driving spoke needs only one DOF. Take the structure symmetry into consideration, a "X" shaped telescopic spoke with only one DOF is used here. As shown in Fig. 9(a), in wheel mode, the telescopic spoke keeps the wheel rim round at the support joint. The track wheels are mounted on the track wheel frame which is coincident with the long axle and coupling jointed with the deformable wheel rim at its ends. When switching to a track, the telescopic spoke changes its length to make the wheel rim deformed (see Fig. 9(b)). Meanwhile, the deformation of the wheel rim elongates the track wheel rim, which also expands out the track wheels to stretch the rubber belt up. Different position of the support joint means different driving force is required for the telescopic spoke to control the shape of the deformable wheel rim. In this section, the driving property of the telescopic spoke is analyzed based on mode switch process modeling of the deformable rim. Then, the position of the support joint is settled and the required driving force of telescopic spoke is figured.

4.1. Mode switch process force modeling

Being composed of four completely identical arc rim segments, the deformable rim can be simplified as one arc rim segment for the kinematic analysis, which would not make any differences. As a single-DOF closed-loop planar linkage, the length variation property of the telescopic spoke can be figured by coordinate transition. As shown in Fig. 10, arc rim $\widehat{AB}$ is supported by spoke OC, whose length l_{O_FC} and angle β change along with the deformation of the foldable rim. When the position of support point C slides along the quadrant, the variation laws of l_{O_FC} and β also change during the mode switch process.

During a mode switch process from Morph-R to Morph-D, the deformation angle α changes from 45° to 0°. The relationship between α, β, β_0, and l_{O_FC} can be described by a kinematic analysis of the deformable rim's transformation process, where $\beta_0 = \angle A_0 O_F C_0 \in [0°, 90°]$ denote the initial angle of $\angle AO_FC$, the value of which depends on the support position of point C. In initial position when the deformable rim is in Morph-R (dashed line), the center of the arc rim segment $\widehat{A_0B_0}$ coincides

https://doi.org/10.1017/S0263574719001589 Published online by Cambridge University Press

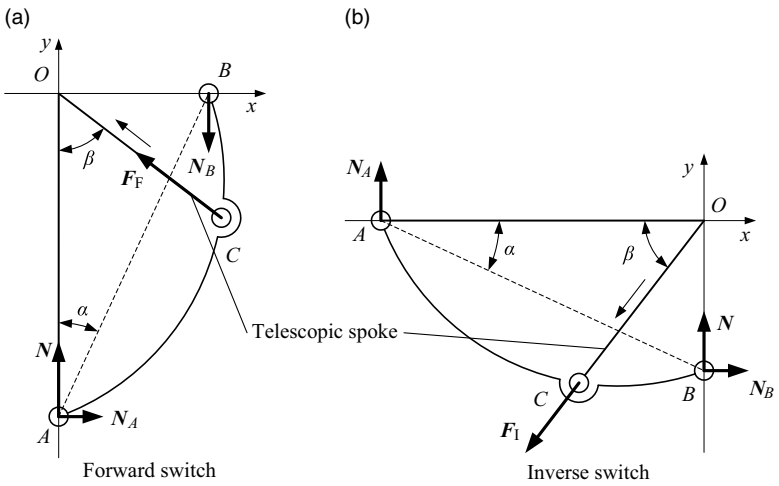

Fig. 11. Force diagram of the mode switch process.

with the origin of rectangular coordinate system $O_F x_F y_F$ which is fixed to the ground. Coordinate axis $O_F x_F$, $O_F y_F$ goes through A_0 and B_0, the two ends of $\widehat{A_0B_0}$, respectively. Moving coordinate system $O_M x_M y_M$ is attached to $\widehat{AB}$. When A_0 and B_0 slide to A and B, respectively, the center of arc rim segment $\widehat{AB}$ translates to O_M, which is described by 2×1 vector $\boldsymbol{o}_M^F$. 2×1 vector $\mathbf{c}^F$ and $\mathbf{c}^M$ represent the coordinate of point C with respect to $O_F x_F y_F$ and $O_M x_M y_M$, respectively. 2×2 matrix $\boldsymbol{R}_M^F$ describes the rotation of $O_M x_M y_M$ related to $O_F x_F y_F$. According to the homogenous conversion formula, there is:

$$\boldsymbol{c}^F = \boldsymbol{R}_M^F \boldsymbol{c}^M + \boldsymbol{o}_M^F \tag{9}$$

where

$$\boldsymbol{c}^M = \begin{bmatrix} R\cos\beta_0 \\ R\sin\beta_0 \end{bmatrix} \tag{10}$$

$$\boldsymbol{R}_M^F = \begin{bmatrix} \cos(45^\circ - \alpha) & -\sin(45^\circ - \alpha) \\ \sin(45^\circ - \alpha) & \cos(45^\circ - \alpha) \end{bmatrix} \tag{11}$$

$$\boldsymbol{o}_M^F = \begin{bmatrix} R\sin(45^\circ - \alpha) \\ -R\sin(45^\circ - \alpha) \end{bmatrix}. \tag{12}$$

Then

$$\boldsymbol{c}^F = R\begin{bmatrix} \cos(45^\circ - \alpha + \beta_0) + \sin(45^\circ - \alpha) \\ \sin(45^\circ - \alpha + \beta_0) - \sin(45^\circ - \alpha) \end{bmatrix}. \tag{13}$$

Therefore, length $l_{O_F C}$ and angle β of the support spoke can be described as:

$$\begin{aligned} l_{O_F C} &= \left|\boldsymbol{c}^F\right| = \sqrt{(\boldsymbol{c}_x^F)^2 + (\boldsymbol{c}_y^F)^2} \\ &= R\sqrt{1 + 2\sin(45^\circ - \alpha)[\sin(45^\circ - \alpha) + \cos(45^\circ - \alpha + \beta_0) - \sin(45^\circ - \alpha + \beta_0)]} \end{aligned} \tag{14}$$

$$\beta = \arctan\frac{\boldsymbol{c}_x^F}{\boldsymbol{c}_z^F} = \frac{\cos(45^\circ - \alpha + \beta_0) + \sin(45^\circ - \alpha)}{\sin(45^\circ - \alpha + \beta_0) - \sin(45^\circ - \alpha)}. \tag{15}$$

Since there is no strict requirement for the switch speed between different modes, the deformation process of the wheel rim can be treated as a quasi-static problem. Therefore, the biggest resistance of the deformation comes from the robot's own gravity.

As shown in Fig. 11, (a) describes the forward switch process during which the wheel rim deforms from Morph-R to Morph-F ($\alpha : 45^\circ \to 0^\circ$), and (b) describes the inverse switch process

https://doi.org/10.1017/S0263574719001589 Published online by Cambridge University Press

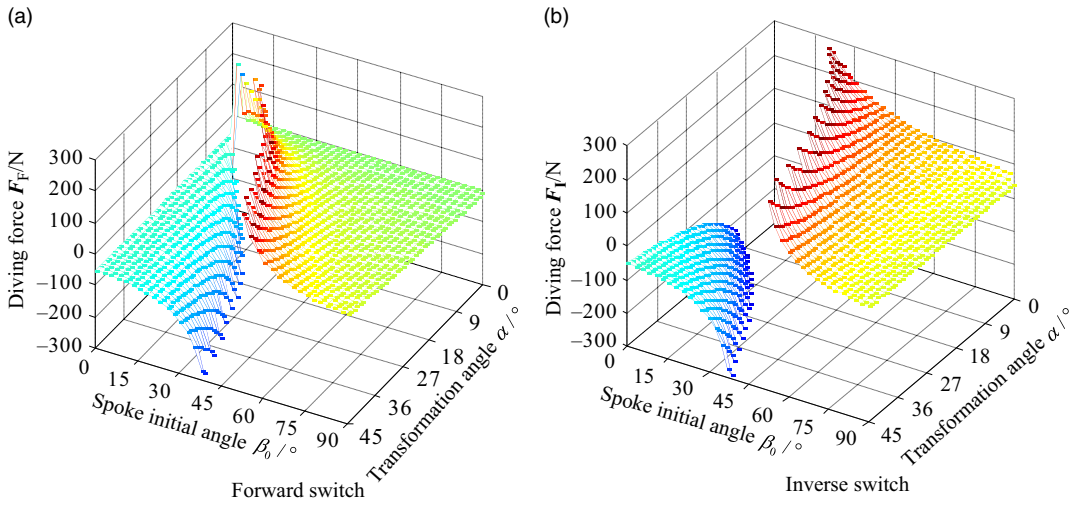

Fig. 12. Simulated driving force of the telescopic spoke.

($\alpha : 0° \rightarrow 45°$). Set N as the outer resistance during the switch process. During the forward switch process, spoke OC rotates to the major axis OA and its angle β decreases. And it is just the opposite during the inverse switch process. The driving force is also available according to the equation of static equilibrium.

For forward switch, there is:

$$\begin{cases} F_{\mathrm{F}} \sin\beta - N_A = 0 \\ F_{\mathrm{F}} \cos\beta + N - N_B = 0 \\ N_A l_{OA} - N_B l_{OB} = 0 \end{cases}. \tag{16}$$

For inverse switch, there is:

$$\begin{cases} F_{\mathrm{I}} \cos\beta - N_B = 0 \\ F_{\mathrm{I}} \sin\beta - N - N_A = 0 \\ N_A l_{OA} - N_B l_{OB} = 0 \end{cases} \tag{17}$$

where N means the reaction force to the gravity from the ground.

Therefore, the driving force can be described as:

$$\begin{cases} F_{\mathrm{F}} = \frac{G l_{OB}}{l_{OA}\sin\beta - l_{OB}\cos\beta}, (\alpha : 45° \rightarrow 0°) \\ F_{\mathrm{I}} = \frac{G l_{OA}}{l_{OA}\sin\beta - l_{OB}\cos\beta}, (\alpha : 0° \rightarrow 45°) \end{cases}. \tag{18}$$

4.2. Driving force and load-bearing analysis

According to Eq. (18), the driving force of the telescopic spoke during a round-trip switch process can be determined, wherein a positive value indicates that the driving force is pulling, and a negative value represents a propulsive movement during the forward switch (see Fig. 12(a)). During the inverse switch, the opposite is true (see Fig. 12(b)). It can be seen that there is a gap in both Fig. 12(a) and (b), which represents the point at which the driving force reaches infinity. On two sides of the gap, the values of the driving force are opposite in sign. This means that the length change of the telescopic spoke is not monotonous, and the inflection point occurs at the gap position. Since the motion direction at the inflection point is uncontrollable, it should be avoided when deciding the position of the spoke's support point. Therefore, the value range of β_0 should be $\beta_0 \in [45°, 90°]$. Moreover, if $\beta_0 = 0°$, the inflection point appears at the state $\alpha = 0°$ when the deformable rim is completely folded. Therefore, $\beta_0 = 0°$ is also an available option as long as the deformable rim is not folded completely (i.e., B and B' do not coincide).

Since the wheel rim is divided into separate arc rim segments, its stiffness and strength are inevitably weakened compared to those of a full wheel rim. In addition to driving the deformation of

https://doi.org/10.1017/S0263574719001589 Published online by Cambridge University Press

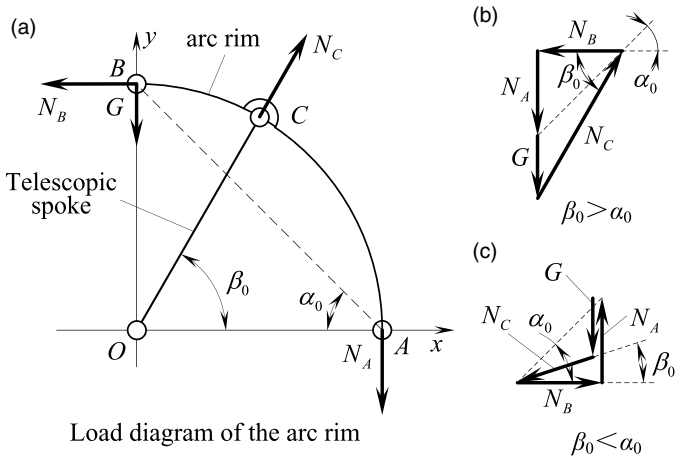

Fig. 13. Load-bearing force diagram of the deformable rim.

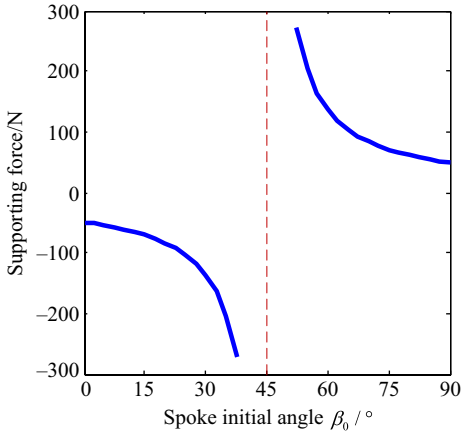

Fig. 14. Supporting force with different initial angles.

the wheel rim, the telescopic spoke also has a supporting role in improving the load-bearing capacity of the deformable rim. As shown in Fig. 13, when the deformable rim is subjected to external pressure, the telescopic spoke should provide supporting force for the deformable rim to maintain a round shape in the Morph-R configuration.

In wheel mode, the action point of external force (gravity or impact from the ground) changes along the circumference of the deformable rim with the rotation of the wheel. The weakest position of the deformable rim is the hinge point between the arc rim segments. Therefore, the case where gravity acts on rim hinge point B is analyzed (Fig. 13(a)). If the initial angle of the telescopic spoke $\beta_0 > \alpha_0 = 45°$, the telescopic spokes provide thrust (Fig. 13(b)). If $\beta_0 < \alpha_0 = 45°$, the telescopic spokes provide tension (Fig. 13(c)).

Supposing that each reconfigurable wheel bears a load of 5 kg, the curve of the required supporting force to keep the deformable rim round with different initial angles of the telescopic spoke is shown in Fig. 14. The lower the supporting force required, the better the load-bearing ability of the deformable rim. It can be seen that the closer the initial angle of the telescopic spoke β_0 is to 45°, the larger the supporting force required. This law is consistent with the above change law of mode switch driving force (see Fig. 12(a) and (b), set $\alpha_0 = 45°$). Therefore, when choosing the initial angle of the telescopic spoke, $\beta_0 = 0°$ or 90° is recommended. According to the mode switch driving force and load-bearing ability analysis in this section, the telescopic spoke with initial angle $\beta_0 = 90°$ seems to be the best choice. However, when $\beta_0 = 90°$, the telescopic spoke is coincide with the minor axis. In this situation, the telescopic spoke is supposed to shorten from R to 0. The magnification ratio is so large that it is quite difficult to realize by mechanism. Therefore, the telescopic spoke with initial

https://doi.org/10.1017/S0263574719001589 Published online by Cambridge University Press

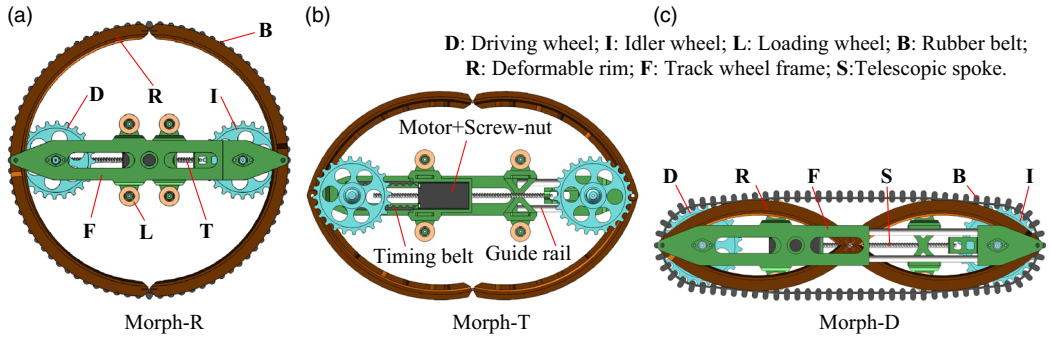

Fig. 15. Mechanical structure of the reconfigurable wheel.

angle $\beta_0 = 0°$ is chosen as the mode switch driving mechanism, with a constraint that the deformable rim should not be folded completely.

5. Experiment Results and Discussion

In Sections 2–4, the configuration of the deformable rim, the caterpillar loop, and the telescopic spoke, which are the three key components of the reconfigurable wheel, were analyzed and settled. According to the results of above study, the design of the reconfigurable wheel is accomplished (see Fig. 15), combining the caterpillar loop configuration with two ends on the ground and the telescopic spoke with an initial angle of $\beta_0 = 0°$. The detailed design process is presented in our previously published paper.[34] $\beta_0 = 0°$ represents that the telescopic spoke is also coincided with the major axis of the deformable rim. Therefore, the telescopic spoke is coaxial with the track wheel frame (see Fig. 15). During the mode switch process, the telescoping of the spoke is driven by a screw-nut mechanism which is powered by a motor (see Fig. 15(b)). Meanwhile, the track wheel frame stretches along with the telescopic spoke.

5.1. Mode switch test of the reconfigurable wheel

Based on the above structure design, a prototype of the reconfigurable wheel was fabricated by 3D printing. Each reconfigurable wheel has three driving motors: two for locomotion driving and one for mode switch driving. In wheel mode and leg mode (see Fig. 16), the reconfigurable wheel is driven by the same transmission system, in which the whole deformable rim rotates with respect to the output shaft. The only difference is the shape of the deformable rim, which is round in wheel mode and folded in leg mode. Thus, the reconfigurable wheel uses the same locomotion driving motor in the above two modes. In track mode (see Fig. 15(b)), the other locomotion driving motor drives the track driving wheel through a timing belt transmission. During the forward switch process, the reconfigurable wheel switches from a round wheel to a vertical leg (see Fig. 16(c)), which takes 5 s. During the inverse switch process, the reconfigurable wheel switches from a flat track to a round wheel (see Fig. 16(d)), which also costs 5 s.

The driving force of the telescopic spoke during a round-trip mode switch process is shown in Fig. 17.

It can be seen that the driving force remains unchanged during the transformation process and monotonically decreases during the inverse switch process, which is consistent with the above change law of mode switch driving force (see Fig. 12(a) and (b), set $\alpha_0 = 45°$). This means that the closer the rim shape is to Morph-F, the larger the mode switch driving force required. A extreme case happens when the rim is completely folded (see Fig. 6(c), B and B' coincide, when $\alpha = 0°$); the driving force required for the transformation is infinite, which means it is a motion dead point and should be avoided. Therefore, the rim cannot be completely folded during the transformation to track mode or leg mode to ensure the smooth implementation of the mode switch.

5.2. Load-bearing and locomotion test

A load-bearing test was also conducted on the deformable rims of the 3D-printed prototype (see Fig. 18). The track wheel frame, which elongates with the folding of the deformable rim, coincided with the major axis of the deformable rim. A load of 5 kg acted in the vertical direction to simulate

https://doi.org/10.1017/S0263574719001589 Published online by Cambridge University Press

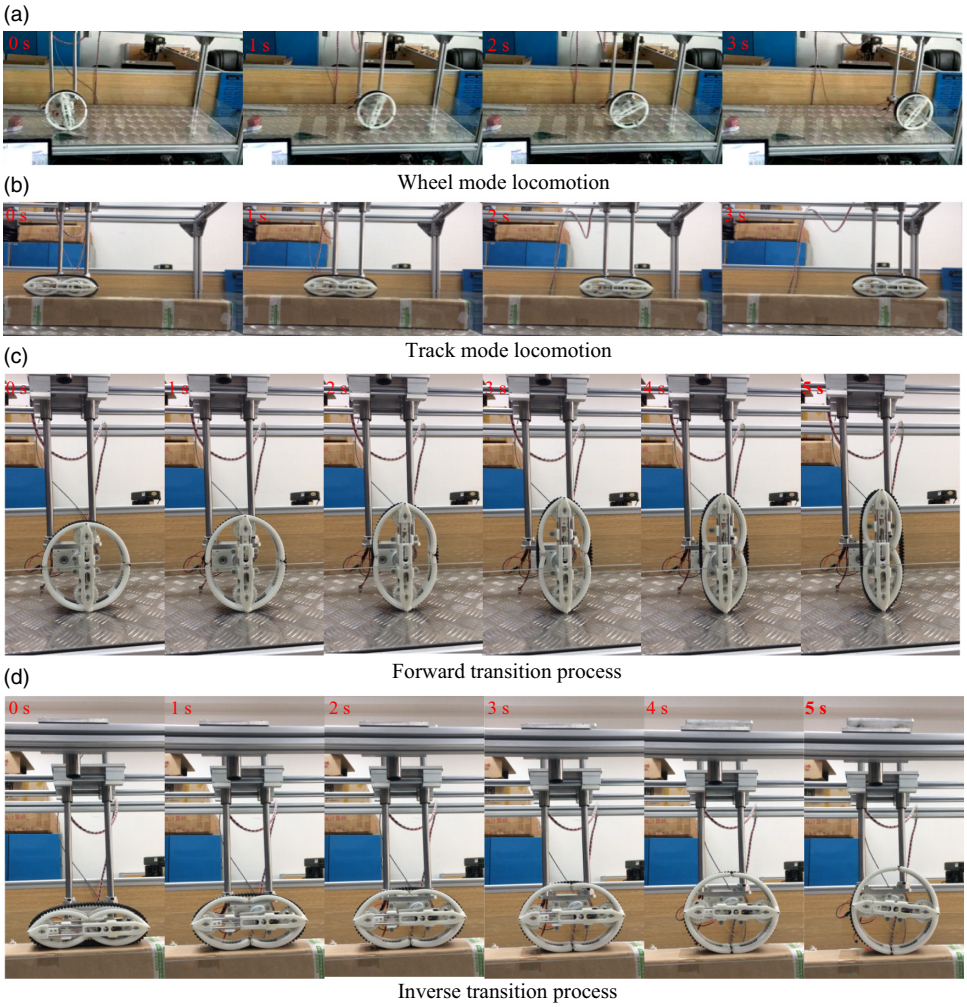

Fig. 16. Mode switch test of the reconfigurable wheel.

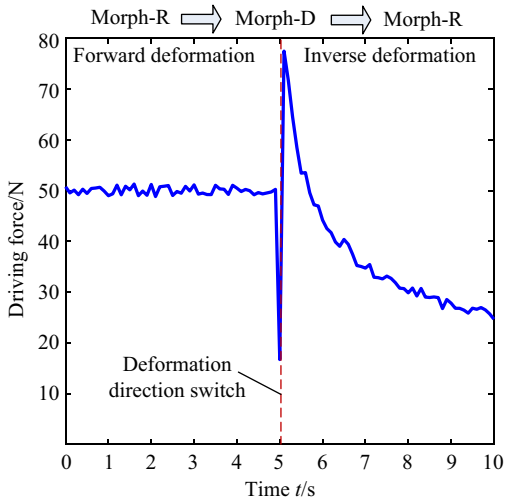

Fig. 17. Tested driving force of the telescopic spoke.

https://doi.org/10.1017/S0263574719001589 Published online by Cambridge University Press

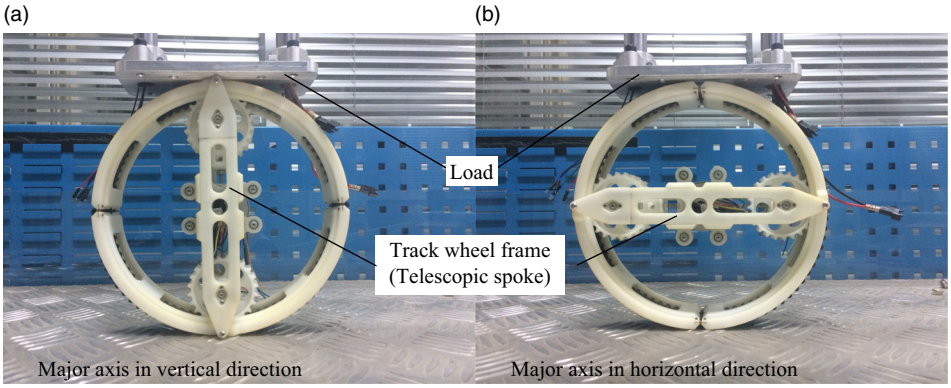

Fig. 18. Load-bearing test of the telescopic spoke.

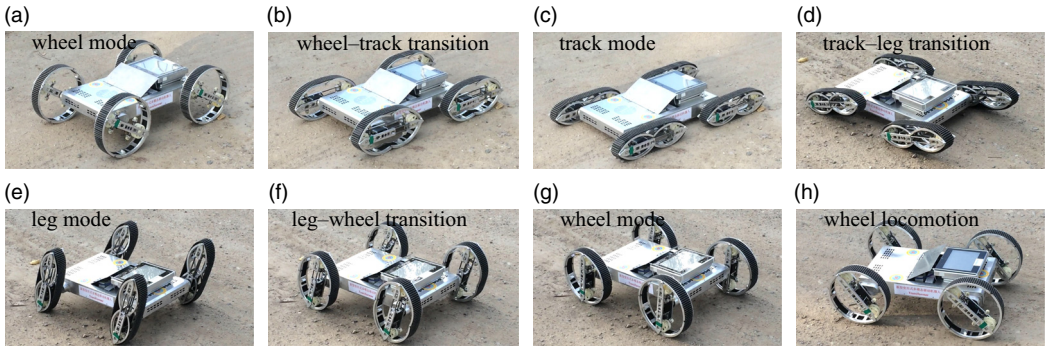

Fig. 19. Reconfigurable robot with multimodal locomotion.

gravity and impact, and the deformable rim was tested in two directions. It can be seen that the deformable rim can bear the load and rarely deforms in both the vertical direction and the horizontal direction.

According to above tests conducted on the prototype of the reconfigurable wheel, the locomotion function in different modes, the configuration switch between different modes, and the load-bearing ability of the configuration design were verified. Thus, a prototype of the reconfigurable robot was manufactured by CNC machining (see Fig. 19) based on the structure of the reconfigurable wheel. By folding or unfolding the deformable rim, the reconfigurable robot can achieve different locomotion modes—when the deformable rim is round (Morph-C), the robot works in wheel mode (see Fig. 19(a)); when the deformable rim begins to transform (Morph-T, see Fig. 19(b)), the robot can switch from wheel mode to track mode (see Fig. 19(c)); when the flat track rotates to stand up (see Fig. 19(d)), the robot can switch from track mode to leg mode (see Fig. 19(e)); and finally, the folded rim can unfold and switch back (see Fig. 19(f)) to wheel mode and keep running (see Fig. 19(g) and (h)). According to the test results, the wheel mode speed can reach 3 m/s, the track mode can reach 1.5 m/s, and the leg mode can reach 1 m/s. The switch between different locomotion modes takes 10 s.

6. Conclusion and Future Works

In this paper, we focused on the configuration design of a reconfigurable robot which merges the functions of wheels, tracks, and legs together. A deformable rim was utilized to make the robot wheel reconfigurable in order to change its locomotion mode. Three rules of configuration design to achieve reconfiguration between different modes were proposed: (1) in wheel mode, the track wheel set should be hidden inside the wheel rim; (2) in track/leg mode, the folded wheel rim should be hidden inside the track ring; (3) the circumference of the wheel rim in wheel mode should be equal to the length of the track ring in track mode. According to these rules, the configuration of the deformable rim, track wheel set, and telescopic spoke were analyzed and designed. A prototype of the reconfiguration wheel was fabricated by 3D printing, and its functions of locomotion in different modes, the switch between different modes, and its load-bearing ability were tested. The results of

https://doi.org/10.1017/S0263574719001589 Published online by Cambridge University Press

these tests verified the effectiveness of the configuration design. Furthermore, a prototype of the reconfigurable robot was manufactured by CNC machining to verify the structural design of the reconfigurable wheel. By testing, the robot was found to be capable of reaching a speed of 3 m/s in wheel mode, 1.5 m/s in track mode, and 1 m/s in leg mode. The switch between different locomotion modes took 10 s.

Compared to the wheel–track reconfigurable robots mentioned in Section 1,[14–18] neither a variable-length caterpillar band nor a variable-diameter wheel is needed in this configuration, which improves the robot's motion reliability and smoothness. Compared to the wheel–leg reconfigurable robots mentioned in Section 1,[19–27] the configuration design in this paper provides the robot with an additional locomotion mode—track mode—which can improve its ability to move on swampy and slippery terrains. Compared to traditional hybrid robots with individual wheels, tracks, and legs,[9–13] this configuration design utilizes a single mechanism to achieve multimodal locomotion, combining flexible mobility and structure compactness together. It can be widely used as a universal mobile platform in SAR and EOD missions.

Currently, we have only implemented the fabrication and basic function of the reconfigurable robot. In the future, we will focus on the study of motion planning and control strategy of the robot on variable grounds. For example, on flat and firm roads, wheel mode is preferred to achieve high speed and efficiency. On swampy and slippery terrain, track mode can provide a better traversing ability. Lastly, leg mode can be used to climb up stairs and step over obstacles on rough roads. With sensors such as cameras and radars as well as navigation devices, we hope to enhance the robot's environmental awareness to improve its terrain adaptability and autonomy.

Acknowledgements

We would like to thank the Laboratory Engineer Tong Cai for his hard work in the processing, assembly, and commissioning of the prototype. Thanks to Lab Assistant Yukang Chang for his help in the control system of the robot.

Funding

This research was funded by the National Natural Science Foundation of China (Grant NO. 51575519, NO. 51675522, NO. 51675524, NO. 51705525, and NO. 51705524) and the Natural Science Foundation of Hunan Province, China (Grant NO. 2017JJ3355).

Conflicts of Interest

The authors declare no conflict of interest. The funders had no role in the design of the study; in the collection, analyses, or interpretation of data; in the writing of the manuscript, or in the decision to publish the results.

References

1. L. Bruzzone and G. Quaglia, "Review article: Locomotion systems for ground mobile robots in unstructured environments," *Mech. Sci*. **3**(2), 49–62 (2012).
2. T. Ylikorpi and J. Suomela, "Ball shaped robots: An historical overview and recent development at TKK," *Field Serv. Rob*. **25**(6), 343–354 (2006).
3. Y. Tian, Y.-A. Yao, W. Ding and Z. Xun, "Design and locomotion analysis of a novel deformable mobile robot with worm-like, self-crossing and rolling motion," *Robotica* **33**(1), 1–18 (2014).
4. D. F. Hougen, S. Benjaafar, J. C. Bonney, J. R. Budenske, M. Dvorak, M. Gini, H. French, D. G. Krantz, P. Y. Li and F. Malver, "A Miniature Robotic System for Reconnaissance and Surveillance," *Proceedings of the International Conference on Robotics and Automation*, San Francisco, CA, USA (2000) pp. 501–507.
5. F. Matsuno and S. Tadokoro, "Rescue Robots and Systems in Japan," *Proceedings of the IEEE International Conference on Robotics and Biomimetics*, New Orleans, LA, USA (2004) pp. 12–20.
6. B. M. Yamauchi, "PackBot: A versatile platform for military robotics," *Proc. SPIE* 5422, 228–237 (2004), doi:10.1117/12.538328.
7. R. M. Voyles, A. C. Larson, B. Jaewook and M. Lapoint, "Core-Bored Search-and-Rescue Applications for an Agile Limbed Robot," *Proceedings of the IEEE/RSJ International Conference on Intelligent Robots and System*, Sendai, Japan (2004) pp. 58–63.
8. J. Liu, Y. Wang, B. Li and S. Ma, "Current research, key performance and future development of search and rescue robots," *Front. Mech. Eng. China* **2**(4), 404–416 (2007).
9. J. Kim, Y.-G. Kim, J.-H. Kwak, D.-H. Hong and J. An, "Wheel & Track Hybrid Robot Platform for Optimal Navigation in an Urban Environment," *Proceedings of the SICE Annual Conference*, Taipei, Taiwan (2010) pp. 881–884.

10. K. Hashimoto, T. Hosobata, Y. Sugahara, Y. Mikuriya, H. Sunazuka, M. Kawase, H.-O. Lim and A. Takanishi, "Realization by Biped Leg-Wheeled Robot of Biped Walking and Wheel-Driven Locomotion," *Proceedings of the IEEE International Conference on Robotics and Automation*, Barcelona, Spain (2005) pp. 2970–2975.
11. M. Lawn and T. Takeda, "Design of a Robotic Hybrid Wheel Chair for Operation in Barrier Present Environments," *Proceedings of the IEEE International Conference of the Engineering in Medicine and Biology Society*, Osaka, Japan (2013) pp. 1013–1018.
12. H.-B. Tian, H.-W. Ma, Y.-S. Zhang and W.-F. Shang, "Design and implementation of wheel-tracked mobile robot," *Modular Mach. Tool Autom. Manuf. Tech.* (7), 15–18 (2015).
13. S.-K. Wang, X.-D. Meng and H.-P. Shang, "Design of a wheel-tracked stair-climbing wheelchair," *J. Mech. Transm.* **37**(10), 156–159 (2013).
14. J.-S. Koh, D.-Y. Lee, S.-W. Kim and K.-J. Cho, "Deformable Soft Wheel Robot using Hybrid Actuation," *Proceedings of the IEEE/RSJ International Conference on Intelligent Robots and Systems*, Vilamoura (2012) pp. 3869–3870.
15. D.-Y. Lee, J.-S. Koh, J.-S. Kim, S.-W. Kim and K.-J. Cho, "Deformable-wheel robot based on soft material," *Int. J. Precis. Eng. Manuf.* **14**(8), 1439–1445 (2013).
16. J.-B. Hu, A.-S. Peng, Y.-S. Ou and G.-L. Jiang, "On Study of a Wheel-Track Transformation Robot," *Proceedings of the IEEE International Conference on Robotics and Biomimetics*, Zhuhai, China (2015) pp. 2460–2465.
17. J.-W. Lee, B.-S. Kim and J.-B. Song, "A small robot based on hybrid wheel-track mechanism," *Trans. Korean Soc. Mech. Eng.* **33**(6), 545–551 (2009).
18. J. Qu and W.-B Zhong, "Design and obstacle-surmounting performance analysis of wheel-track transformable wheel," *J. South China Univ. Technol.* **41**(5), 119–124 (2013).
19. J.-J. Chou and L. S. Yang, "Innovative Design of a Claw-Wheel Transformable Robot," *Proceedings of the IEEE International Conference on Robotics and Automation*, Karlsruhe, Germany (2013) pp. 1337–1342.
20. Y. She, C. J. Hurd and H.-J. Su, "A Transformable Wheel Robot with a Passive Leg," *Proceedings of the IEEE/RSJ International Conference on Intelligent Robots and Systems*, Sendai (2015) pp. 4165–4170.
21. K. Tadakuma, R. Tadakuma, A. Maruyama, E. Rohmer, K. Nagatani, K. Yoshida, A. Ming, M. Shimojo, M. Higashimori and M. Kaneko, "Mechanical Design of the Wheel-Leg Hybrid Mobile Robot to Realize a Large Wheel Diameter," *Proceedings of the IEEE/RSJ International Conference on Intelligent Robots and Systems*, Sendai (2010) pp. 3358–3365.
22. Y.-S. Kim, G.-P. Jung, H. Kim, K.-J. Cho and C.-N. Chu, "Wheel Transformer: A Miniaturized Terrain Adaptive Robot with Passively Transformed Wheels," *Proceedings of the IEEE/RSJ International Conference on Robotics and Automation*, Karlsruhe, Germany (2013) pp. 5625–5630.
23. Y.-S. Kim, G.-P. Jung, H. Kim, K.-J. Cho and C.-N. Chu, "Wheel transformer: A wheel-leg hybrid robot with passive transformable wheels," *IEEE Trans. Rob.* **30**(6), 1487–1498 (2014).
24. F. Masataka, R. E. Mohan, N. Tan, A. Nakamura and T. Pathmakumar, "Terrain perception in a shape shifting rolling-crawling robot," *Robotics* **5**(4), 19 (2016). doi:10.3390/robotics5040019.
25. T. Yanagida, R. E. Mohan, T. Pathmakumar and K. Elangovan, "Design and implementation of a shape shifting rolling-crawling-wall-climbing robot," *Appl. Sci.* **7**(4), 342 (2017). doi:10.3390/app7040342.
26. S.-Y. Shen, C.-H. Li, C.-C. Cheng, J.-C. Lu, S.-F. Wang and P.-C. Lin, "Design of a Leg-Wheel Hybrid Mobile Platform," *Proceedings of the IEEE/RSJ International Conference on Intelligent Robots and Systems*, St. Louis, MO (2009) pp. 4682–4687.
27. K.-J. Huang, S.-C. Chen, Y.-C. Chou, S.-Y. Shen, C.-H. Li and P.-C. Lin, "Experimental Validation of a Leg-wheel Hybrid Mobile Robot Quattroped," *Proceedings of the IEEE International Conference on Robotics and Automation*, Shanghai, China (2011) pp. 2976–2977.
28. S.-C. Chen, K.-J. Huang, W.-H. Chen, J.-C. Lu, S.-F. Wang and P.-C. Lin, "Quattroped: A leg-wheel transformable robot," *IEEE/ASME Trans. Mechatron.* **19**(2), 730–742 (2014).
29. H.-S. Lin, W.-H. Chen and P.-C. Lin, "Model-based Dynamic Gait Generation for a Leg-wheel Transformable Robot," *Proceedings of the IEEE International Conference on Robotics and Automation*, (2015) pp. 5184–5190.
30. G. Gogu, "Mobility of mechanisms: A critical review," *Mech. Mach. Theory* **40**(9), 1068–1097 (2005).
31. S. Wakabayashi, H. Sato and S.-I. Nishida, "Design and mobility evaluation of tracked lunar vehicle," *J Terramech*. **46**(3), 105–114 (2009).
32. F.-L. Zhou, H.-J. Xu, T.-A. Zou and X. Zhang, "A Wheel-Track-Leg Hybrid Locomotion Mechanism Based on Transformable Rims," *Proceedings of the IEEE International Conference on Advanced Intelligent Mechatronics*, Munich, Germany (2017) pp. 315–320.
33. A. Bodin, "Development of a tracked vehicle to study the influence of vehicle parameters on tractive performance in soft terrain," *J. Terramech.* **36**(3), 167–181 (1999).
34. F.-L. Zhou, X.-J Xu, H.-J Xu and X. Zhang, "A Multimodal Hybrid Robot with Transformable Wheels," *Proceedings of the IEEE International Conference on Real-time Computing and Robotics*, Okinawa, Japan (2017) pp. 139–144.